Supplementary Material: Effect of Compliance on Morphological Control of Dynamic Locomotion with HyQ

Gabriel Urbain, Victor Barasuol, Claudio Semini, Joni Dambre and Francis wyffels

October 8, 2020

1 Locomotion Metrics

The metrics in this paper aim at providing a behavioral understanding of the locomotion process using quantities that can be compared together across experiments. We adopted the following definitions as they indicated a good representation of the HyQ gait characteristics and correlated well with a qualitative inspection.

1.1 Stability

This concept describes the property of the system to stay in its own limit cycle, despite external disturbance. Stable locomotion induces low oscillation of the trunk in roll, pitch, and height oscillations. The stability is measured by the range between the maximal height of the highest point on the robot's trunk and the minimal height of the lowest point on the trunk during the full test period:

$$S \;=\; \max\left(z_k + \frac{l}{2}\tan(\phi_k) + \frac{L}{2}\tan(\psi_k)\right) \;-\; \min_k\left(z_k + \frac{l}{2}\tan(\phi_k) + \frac{L}{2}\tan(\psi_k)\right) \quad \text{for} \quad k \;\in\; [0,\; t_{\text{test}}], \tag{1}$$

where (x_k, y_k, z_k) is the position of the robot at timestep k; $(\phi_k, \theta_k, \psi_k)$ is the attitude in term of roll, pitch and yaw; l is the width of the robot equal to 0.5 meters and L is the length of the robot (1.3 meters including the roll cage protection).

1.2 Average Power

As we are working with a simulator, we do not intend to accurately determinate the power consumption, which involves a good model of the hydraulic actuators and calorific dissipation during the robot-environment interactions. In the scope of our investigations in morphological computation, we are interested in the power that a perfect equivalent passive system would consume during locomotion. To this goal, we compute a virtual work power by averaging the product of all actuators torque and angular speed:

$$P \;=\; \Big(\sum_k \sum_j \dot{q}_k^{\,j} \;\cdot\; \tau_k^{\,j}\Big) \;/\; \mathrm{K} \quad \text{for} \quad k \;\in\; [0,\; t_{\text{test}}] \text{ and for } \quad j \;\in\; \mathcal{J}, \tag{2}$$

where $\mathcal{J}$ is the set of twelve robot actuated joints; $\dot{q}_k^{\,j}$ is the joint angular speed of joint j at time step k; $\tau_k^{\,j}$, its measured torque; and K, the number of time steps in the interval $[0,\; t_{\text{test}}]$.

1.3 Average Speed

The robot average speed is only evaluated on the X-axis, as deviations on the Y-axis are undesirable for the controller in this work. We also normalize this value by the desired robot speed to obtain a coefficient that can be easily assimilated to the speed efficiency. It is computed as:

$$V \;=\; \Big(\sum_{k=1}^{\mathrm{K}} \frac{x_k - x_{k-1}}{t_k - t_{k-1}}\Big) \;/\; \Big((\mathrm{K} \;-\; 1)\;.\;\mathrm{V_d}\Big), \tag{3}$$

where $\mathrm{V_d}$ is the desired velocity of the robot, set to 0.25 m/s in this work.

1.4 Cost of Transport

The Cost of Transport (COT) is the ratio of the power and speed of the robot, normalized by its weight (in Newtons). It is given by:

$$COT \;=\; \frac{P}{V \;.\; m \;.\; g}, \tag{4}$$

where m is the robot mass and g, the gravitational constant. This equation is in line with the definition of Tucker (1975) where the locomotion gaits of several animals and vehicles have been classified in function of their COT.

1.5 Maximal Ground Reaction Forces

The GRFs are used as an input for the closed-loop neural network in the experiments. They play a role to regulate the phase of the gait, by detecting collisions between the foot and the ground, but also to modulate the swing phase when the weight distribution on the four legs is different. In this context, we only keep the component normal to the ground to reduce the dimensionality of the GRF. To quantify the impacts of the robot with the ground during a full experiment, we are only interested in the maximal GRF on the four legs during that period of time:

$$GRF_{\max} \;=\; \max\,\left(\,\mathrm{abs}(GRF\,{}_k^i)\,\right) \quad \text{for} \;\; k \;\in\; [0,\; t_{\text{test}}] \;\text{and for} \quad i \;\in\; \mathcal{L}, \tag{5}$$

With $\mathcal{L}$ the set of right front, left front, right hind, and left hind legs.

1.6 Prediction Accuracy

This accuracy is an indicator to estimate the capacity of the closed-loop system to predict the target signal with the lowest error. We employ the inverse of the Normal Root Mean Square Error (NRMSE) to assess this quality:

$$A \;=\; \sqrt{\frac{\left(\max(q_k^j) - \min(q_k^j)\right)}{(q_k^j - \hat{q}_k^j)^2}} \qquad \text{for } k \;\in\; [0,\; t_{\text{test}}] \text{ and for } j \;\in\; \mathcal{J}. \tag{6}$$

The higher the accuracy, the smaller the error between the target and the prediction.

1.7 Average Training Time Step

The average training time step of the controller gives a good first approximation of the computational requirements of the controller. Unfortunately, it depends on the programming language, the code implementation, the hardware characteristics, and the operating system load. This is why it is not thoroughly analyzed in the paper but a few words are given later in this document. It can be measured as:

$$T \;=\; \frac{\sum_{k=0}^{\mathrm{K}} \; t_k}{t_{\mathrm{K}} - t_0} \tag{7}$$

1.8 Locomotive Cycle

The walking mechanism can be graphically represented by a closed curve called a locomotive cycle and which shows the trajectory of the foot position during a full cycle. It provides information about the length of the stance and swing phases, the liftoff and touch-down times, but also the step height and length (or stride). It generally has the shape of a semi-ellipse, flat on the ground but with higher vertical acceleration for the lift than the touch-down, to increase the step height and avoid high impacts with the ground. To represent this curve and its variability, we simply draw the complete trajectory in a two-dimensional X-Z plane in the frame of reference of the robot trunk.

2 Extended Results for COT at Different Compliance

This section provides an extended analysis of the COT evolution in closed-loop locomotion, even at very high stiffnesses. While Fig. 8 in the main manuscript only presents the essential results to better promote the message, Fig. 1 in this document exhibits a broader range on the X-axis. It also provides additional metrics to interpret the changes in power consumption and speed along with compliance.

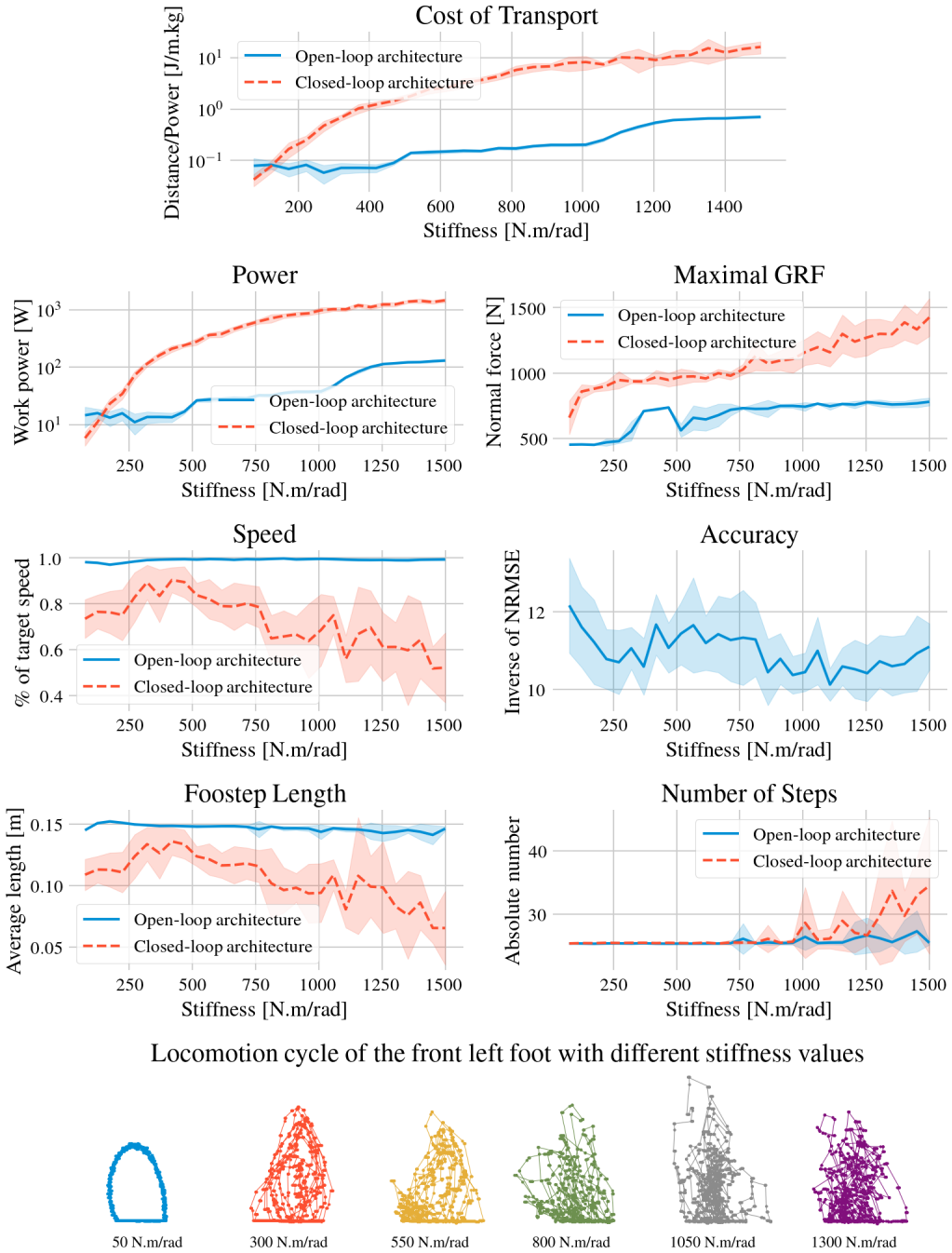

Figure 1: This figure is an extension of Fig. 8 in the main manuscript. It carries the analysis on a broader X-axis to verify that the conclusions are still holding, and provides additional metrics to discuss the behavior of robot locomotion at different stiffnesses.

In the first row of Fig. 1, we observe that the exponential growth of the COT starts to saturate at very high stiffness. This effect is explained by the power graph in the second row and the fact that the torque and speed of the joints cannot grow indefinitely at high stiffness. Although it keeps increasing, the maximal GRFs plotted in the same row also remain in the same order of magnitude at high stiffness.

In the third row, we can notice that the decreasing trend in the robot's speed for stiffer robots, already discussed in the main manuscript, continues with a similar evolution at higher stiffness. A look at the fourth row shows that it correlates principally with a reduction average step length. As suggested by the representation of the locomotion cycles in the last row, oscillations around the main attractor are leading to a reduced step size, which affects the final speed of the robot. Despite these oscillations, we can note that the neural network can track the target even at high stiffness, as the accuracy presented on the third line of Fig. 1 remains in a similar range along the X-axis.

3 Extended Results for the Trade-offs between Controller Complexity and Compliance

In this section, we provide additional data to understand the trade-offs between the controller's complexity and compliance in morphological closed-loop control. The results are displayed in Fig. 2 and constitute an extension of Fig. 9 in the main manuscript. Similarly to the previous section, the representation in the main manuscript is condensed to keep the focus on the main goals of the study, but we provide a larger overview in this document. These additions include the results for a very stiff robot in the third column in Fig. 2 and new metrics in the rows four to six, to evaluate the behavioral aspects of the gait and the complexity of training the controller.

Backing up the discussions in the main manuscript, the third column in Fig. 2 further demonstrates the spreading of the locomotion speed and stability on the graphs when increasing the stiffness. The fourth row represents the maximal impacts between the robot's feet and the ground. A comparison with the stability row just above exhibits a correlation between these two metrics. A simple explanation is that the undesired impacts with the ground are destabilizing the robot. The fifth row represents the power consumption of the robot. It shows that the controller memory and non-linearities have only little impact on consumption, which is mainly driven by compliance. The average training time step represented in the last row only depends on the architecture and has no relation with the robot morphology. There are three clear areas on the graphs, certainly corresponding to different implementation or optimization in the underlying algebra libraries. It is important to note that the controller has not been optimized and better values could be expected with a different implementation. On the computer used for the simulation, only the robot with the *compliant* parameters could be trained to reach a good accuracy at a minimum of 250 Hz, which corresponds to the default frequency used on the real robot. This was taken into account when selecting a neural architecture in the experimental phase with the real robot. Nonetheless, in the testing phase, it is easy to quantify the number of operations in the feed-forward neural network. The number of weighted sums computed by this network is equal to:

$$M \,.\, N \,.\, 5 \;+\; N \,.\, 16, \tag{8}$$

where M and N are respectively the sizes of the delay line and the hidden layer of the controller, as explained in the main manuscript. The number 5 corresponds to the dimension of the input vector and 16, the dimension of the output vector. Further work could explore how this computational performance compares with a traditional implementation of a CPG and solving inverse kinematics.

References

Tucker, V. A. (1975). The energetic cost of moving about: walking and running are extremely inefficient forms of locomotion. much greater efficiency is achieved by birds, fish—and bicyclists. *American Scientist*, *63*(4), 413–419.

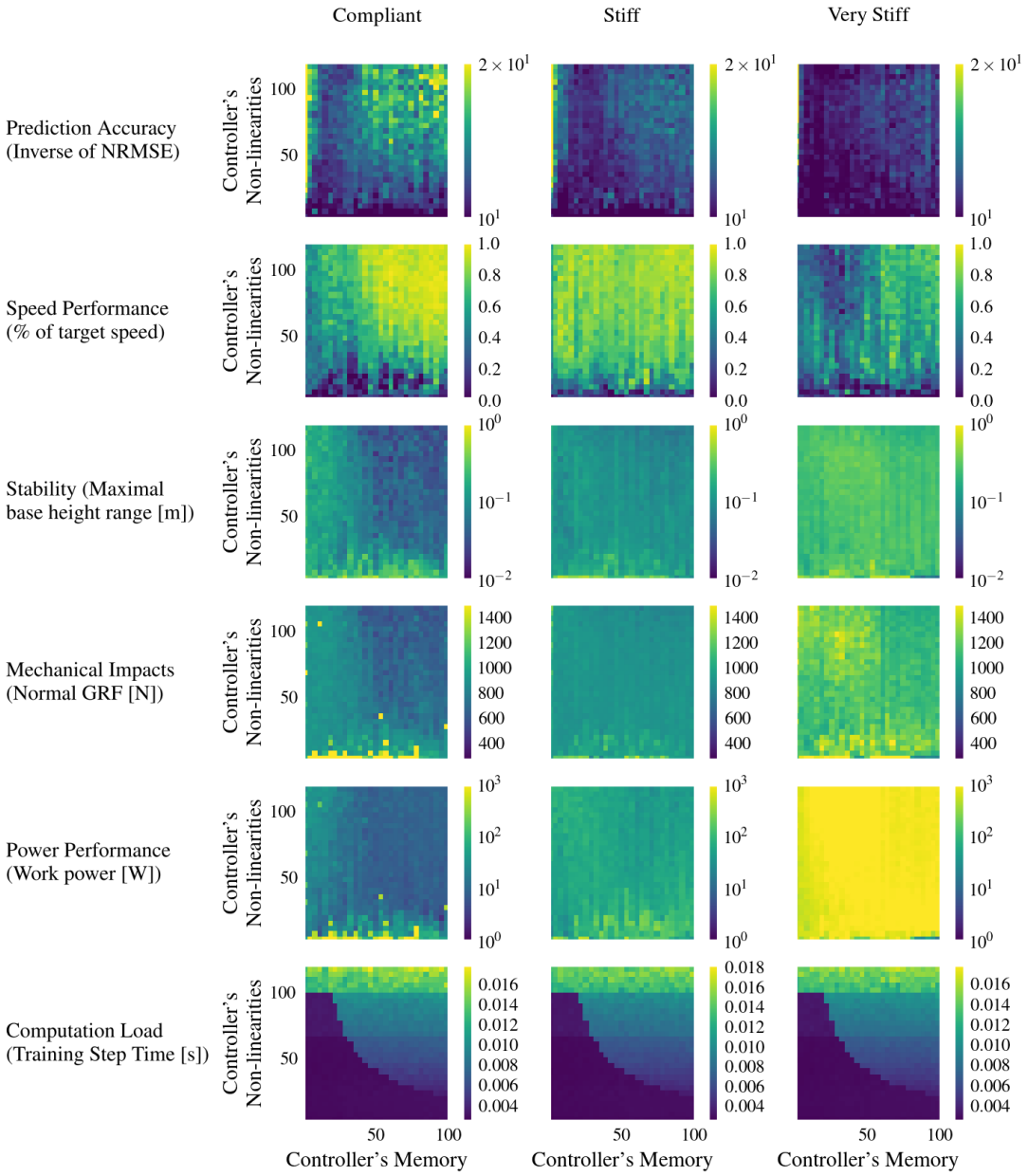

Figure 2: This figure is an extension of Fig. 8 in the main manuscript. We added a third column to validate our discussions at very high stiffness and three new rows with new metrics to better grasp the behavior of the robot. In each graph, the X-axis represents the parameter M, the size of the delay line buffer (memory) and the Y-axis the parameter N, the size of the hidden layer (non-linearities).